

An Electron Fixed Target Experiment to Search for a New Vector Boson A' Decaying to e^+e^-

Rouven Essig,¹ Philip Schuster,¹ Natalia Toro,² and Bogdan Wojtsekhowski³

¹*Theory Group, SLAC National Accelerator Laboratory, Menlo Park, CA 94025*

²*Theory Group, Stanford University, Stanford, CA 94305*

³*Thomas Jefferson National Accelerator Facility, Newport News, VA 23606*

(Dated: October 23, 2018)

We describe an experiment to search for a new vector boson A' with weak coupling $\alpha' \gtrsim 6 \times 10^{-8} \alpha$ to electrons ($\alpha = e^2/4\pi$) in the mass range $65 \text{ MeV} < m_{A'} < 550 \text{ MeV}$. New vector bosons with such small couplings arise naturally from a small kinetic mixing of the “dark photon” A' with the photon — one of the very few ways in which new forces can couple to the Standard Model — and have received considerable attention as an explanation of various dark matter related anomalies. A' bosons are produced by radiation off an electron beam, and could appear as narrow resonances with small production cross-section in the trident e^+e^- spectrum. We summarize the experimental approach described in a proposal submitted to Jefferson Laboratory’s PAC35, PR-10-009 [1]. This experiment, the A' Experiment (APEX), uses the electron beam of the Continuous Electron Beam Accelerator Facility at Jefferson Laboratory (CEBAF) at energies of $\approx 1\text{--}4 \text{ GeV}$ incident on $0.5\text{--}10\%$ radiation length Tungsten wire mesh targets, and measures the resulting e^+e^- pairs to search for the A' using the High Resolution Spectrometer and the septum magnet in Hall A. With a ~ 1 month run, APEX will achieve very good sensitivity because the statistics of e^+e^- pairs will be $\sim 10,000$ times larger in the explored mass range than any previous search for the A' boson. These statistics and the excellent mass resolution of the spectrometers allow sensitivity to α'/α one to three orders of magnitude below current limits, in a region of parameter space of great theoretical and phenomenological interest. Similar experiments could also be performed at other facilities, such as the Mainz Microtron.

I. INTRODUCTION

The development of the Standard Model of particle interactions is the culmination of a century of searches and analyses with fixed-target and colliding beam experiments. Interactions with new forces beyond the Standard Model are currently limited by well-tested gauge symmetries to a handful of possibilities. One of the few remaining ways for interactions with new sub-GeV vector-like forces to arise is for charged particles to acquire millicharges, ϵe , under these forces. This occurs through a simple and generic mechanism proposed by Holdom [2], in which a new vector particle A'_μ mixes via quantum loops with the Standard Model photon. MeV–GeV masses for the A' gauge boson are particularly well-motivated in this context. Such sub-GeV forces are a common feature of extensions of the Standard Model, but existing constraints are surprisingly weak, with limits at $\epsilon e \lesssim (0.3 - 1) \times 10^{-2} e$.

Fixed-target experiments with high-intensity electron beams and existing precision spectrometers are ideally suited to explore sub-GeV forces by probing reactions in which a new A' vector particle is produced by radiation off an electron beam [3, 4]. The A' can decay to an electron and positron pair and appears as a narrow resonance of small magnitude in the invariant mass spectrum. The production rate of A' s, the luminosity, and the mass res-

olution attainable at, for example, Jefferson Laboratory (JLab), the Mainz Microtron, and the SLAC National Accelerator Laboratory vastly exceeds what is currently available using colliding electron beam facilities. In [3], several fixed-target experimental strategies were outlined to search for new sub-GeV vector interactions. In this paper, we summarize a concrete A' search using Jefferson Laboratory’s Continuous Electron Beam Accelerator Facility (CEBAF) and the High Resolution Spectrometers (HRS) in Hall A [1], highlighting the features that are applicable to similar experimental facilities. This experiment, the A' Experiment (APEX), can probe charged particle couplings with new forces as small as $2 \times 10^{-4} e$ and masses between 65 MeV and 550 MeV — an improvement by more than two orders of magnitude in cross section sensitivity over all previous experiments.

Fixed-target experiments of this form are particularly timely in light of a series of recent anomalies from terrestrial, balloon-borne, and satellite experiments that suggest that dark matter interacts with Standard Model particles. Much of this data sharply hints that dark matter is directly charged under a new force mediated by an A' and not described by the Standard Model. Theoretical as well as phenomenological expectations suggest an A' mass $m_{A'} \lesssim 1 \text{ GeV}$ and $\epsilon e \lesssim 10^{-2} e$.

In this paper, we shall focus on a search for new vector bosons. However, it should be emphasized that this

experiment will provide a powerful probe for *any* new particle — vector, pseudo-vector, scalar, or pseudo-scalar — that has sub-GeV mass and couples to electrons (for other collider, accelerator, and direct and indirect astrophysical probes see [5–25]; a proposal for an electron beam incident on a diffuse Hydrogen gas target using the Jefferson Laboratory’s Free Electron Laser has been discussed in [12]).

A. Brief overview of the experimental strategy

The goal of the experiment is to measure the invariant mass spectrum of electron-positron pairs produced by electron scattering on a high- Z target, and search for a narrow peak with width corresponding to the instrumental resolution. The electron and positron are detected in magnetic spectrometers with acceptance over a small range of particle momentum and angle, such that each experimental setting is sensitive to a mass window $\sim \pm 30\%$ about a central mass value. Using four beam energies from 1–4 GeV, APEX will scan the e^+e^- spectrum in the mass range 65 MeV to 550 MeV.

Optimal sensitivity for these masses is achieved by studying symmetric e^+e^- kinematics, where each particle carries approximately half the beam energy and has an opening angle ≈ 5 deg relative to the beam. Such small effective angles for the spectrometer can be achieved using a septum magnet [1, 26]. Without a septum magnet, lower beam energies and correspondingly wider angles could be used to probe the same mass range. The impact of the geometry on the physics reach will be reviewed in §III and was discussed in detail in [3].

The experimental sensitivity is determined by statistics and mass resolution. Given the precision of spectrometers used, the latter is limited by multiple scattering in the target material. In APEX, a long, tilted wire mesh target is used to obtain excellent relative mass resolution of 0.5%. In addition, different segments of the target will enter the spectrometers for different central angles, increasing the size of mass window probed by each setting.

With a beam of 80 μA on 0.5%–10% radiation-length targets at various beam energies, we expect to collect true coincidence e^+e^- events with a rate in the range 100–500 Hz (the expected background and accidental coincidence rates within a 2 ns timing window are about an order of magnitude lower). The total e^+e^- sample size will exceed 10^8 pairs in a 6-day period for each setting, or a 12-day period for the 4 GeV setting.

While this paper reflects an experimental setup optimized for the equipment in Hall A at JLab, many of the experimental considerations are also applicable for equipment available at the Mainz Microtron, JLab Hall B, and other experimental facilities.

B. Expected reach and impact

APEX will be sensitive to new gauge bosons with couplings as small as $\alpha'/\alpha \sim (6 - 8) \times 10^{-8}$ for masses in the range 65 – 300 MeV, and couplings as small as $\alpha'/\alpha \sim 2 \times 10^{-7}$ for larger $m_{A'} \lesssim 525$ MeV. This is about a factor of $\sim 3 - 35$ times lower in ϵ than existing constraints (which assume that the A' couples also to muons), and corresponds to $\sim 10 - 1000$ times smaller cross-sections.

The precise mass range probed by this type of experiment can be varied by changing the spectrometer angular settings and/or the beam energies. Thus, other experimental facilities may be able to perform experiments similar to APEX, but targeting complementary regions of parameter space.

The parameter range probed by APEX is interesting for several reasons. This region of mass and coupling is compatible with A' ’s explaining the annual modulation signal seen by the dark matter direct detection experiment DAMA/LIBRA, and also with dark matter annihilating into A' ’s, which explains a myriad of recent cosmic-ray and other astrophysical anomalies (see §II B). In addition, and independently of any connection to dark matter, the proposed experiment would be the first to probe A' ’s of mass $\gtrsim 50$ MeV with gauge kinetic mixing below $\epsilon \sim 10^{-3}$, the range most compatible if the Standard Model hypercharge gauge force is part of a Grand Unified Theory.

The importance for fundamental physics of discovering new forces near the GeV scale cannot be overstated.

C. The organization of this paper

The paper is organized as follows. In §II, we present the physics of hypothetical A' particles, motivation for their existence, current limits, and estimated sensitivity for *potential* future analyses of existing data. In §III, we describe A' production in fixed-target experiments. In §IV, we describe the experimental setup. In §V, we present the parametrics and the Monte Carlo (MC) simulations of the QED e^+e^- pair production rate and the A' signal rate in the proposed setup. We also describe how we made the sensitivity plots. Other background rates, such as π^+ or e^+ singles and accidental e^+e^- pairs, are discussed in §VI. The expected sensitivity is discussed in §VII. The paper is summarized in §VIII. Three appendices discuss the form factors used to calculate the signal and background rates (§A), the mass resolution (§B), and the validation of the rates we obtain with the various MC simulations (§C).

II. PHYSICS

We consider new sub-GeV mass vector bosons — ‘dark photons’ A' — that couple very weakly to electrons

(as mentioned previously, similar considerations apply to pseudo-vectors, scalars, and pseudo-scalars with sub-GeV mass that couple to electrons). It is useful to parameterize the coupling g' of the A' to electrons by a dimensionless $\epsilon \equiv g'/e$, where e is the electron charge. Cross-sections for A' production then scale as $\alpha'/\alpha = \epsilon^2$, where $\alpha' = g'^2/(4\pi)$ and $\alpha = e^2/(4\pi)$ are the fine-structure constants for the dark photon and ordinary electromagnetic interactions, respectively. This experiment will search for A' bosons with mass $m_{A'} \sim 65 \text{ MeV} - 550 \text{ MeV}$ and $\alpha'/\alpha \gtrsim 6 \times 10^{-8}$, which can be produced by a reaction analogous to photon bremsstrahlung (see §III) and decays promptly to e^+e^- or other charged particle pairs. We refer the reader to Figure 1 for a summary of the reach of this experiment.

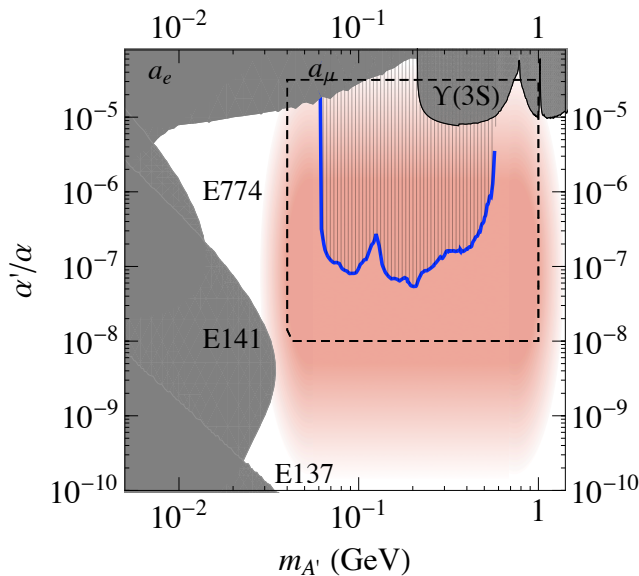


FIG. 1: Anticipated 2σ sensitivity in $\alpha'/\alpha = \epsilon^2$ for the A' experiment (APEX) at Hall A in JLab (thick blue line), with existing constraints on an A' from electron and muon anomalous magnetic moment measurements, a_e and a_μ (see [27]), the BaBar search for $\Upsilon(3S) \rightarrow \gamma\mu^+\mu^-$ [28], and three beam dump experiments, E137, E141, and E774 [29–31] (see [3]). The a_μ and $\Upsilon(3S)$ limits assume equal-strength couplings to electrons and muons. The red region indicates the region of greatest theoretical interest, as described in the text. The gray dashed line indicates the scale used for other plots in this paper. The irregularity of the reach is an artifact of combining several different run settings (see Table II). The precise mass range probed by this type of experiment can be varied by changing the spectrometer angular settings and/or the beam energies. We stress this point as other experimental facilities may be able to perform experiments similar to APEX, but targeting complementary regions of parameter space.

A. Motivation for New Physics Near the GeV Scale

New light vector particles, matter states, and their associated interactions are ubiquitous in extensions of the Standard Model [2, 32–40]. However, the symmetries of the Standard Model restrict the interaction of ordinary matter with such new states. Indeed, most interactions consistent with Standard Model gauge symmetries and Lorentz invariance have couplings suppressed by a high mass scale. One of the few unsuppressed interactions is the coupling of charged Standard Model particles ψ

$$\delta\mathcal{L} = g' A'_\mu \bar{\psi} \gamma^\mu \psi \quad (1)$$

to a new gauge boson A' , which is quite poorly constrained for small g' (see Figure 1)[3]. Similar couplings between the A' and other Standard Model fermions are also allowed, with relations between their couplings (anomaly cancellation) required for the A' gauge symmetry to be quantum-mechanically consistent. For example, the A' can couple only to electrons and muons, with opposite charges $g'_e = -g'_\mu$ (a $U(1)_{e-\mu}$ boson), or can have couplings proportional to the electromagnetic charges q_i of each fermion, $g_i = \epsilon q_i$.

A' couplings to Standard Model matter with the latter structure can be *induced* by ordinary electromagnetic interactions through the kinetic mixing interaction proposed by Holdom [2],

$$\delta\mathcal{L} = \frac{\epsilon_Y}{2} F'_{\mu\nu} F_Y^{\mu\nu}, \quad (2)$$

where $F'_{\mu\nu} = \partial_\mu A'_\nu - \partial_\nu A'_\mu$ is the field strength of the A' gauge boson, and similarly $F_Y^{\mu\nu}$ is the hypercharge field strength. This effect is generic, ensures that the A' interactions respect parity, and (as we discuss below) naturally produces small g' and A' masses near the GeV scale. This mixing is equivalent in low-energy interactions to assigning a charge ϵq_i to Standard Model particles of electromagnetic charge q_i , where $\epsilon = \epsilon_Y/(\cos\theta_W)$ and θ_W is the Weinberg mixing angle. The A' couplings to neutrinos and parity-violating couplings are negligible compared to Z -mediated effects (see e.g. [13]).

As noted in [2], a new gauge boson A' that does not couple to Standard Model matter at a classical level can still couple through quantum-mechanical corrections. For example, loops of any particle X that couples to both the A' and Standard Model hypercharge generates mixing of the form (2), with

$$\epsilon \sim 10^{-3} - 10^{-2} \quad (\alpha'/\alpha \sim 10^{-6} - 10^{-4}). \quad (3)$$

These quantum effects are significant regardless of the mass m_X of the particle in question, which could be well above the TeV scale (or even at the Planck scale) and thus evade detection.

Smaller ϵ are expected if nature has enhanced symmetry at high energies. For example, it has been conjectured that the strong and electroweak gauge groups of the Standard Model are embedded in a grand unified

theory (GUT) with gauge group $SU(5)$ or larger that is broken spontaneously at a high scale $M_G \approx 10^{16}$ GeV. In this case the mixing (2) is suppressed,

$$\epsilon_{GUT} \sim \frac{\alpha_i^2}{16\pi^2} \ln(M_G/M_X) \sim 10^{-5} - 10^{-3}, \quad (4)$$

where α_i are gauge couplings. ϵ of this size leads to effective couplings

$$\alpha'/\alpha \sim 10^{-8} - 10^{-6}. \quad (5)$$

As shown in Figure 1, *no experiment to date has probed the range of ϵ expected in grand unified theories for $m_{A'} \gtrsim 50$ MeV.* (From string theory, the possible range of ϵ is much larger, $\sim 10^{-23} - 10^{-2}$ [35–38].)

An A' mass near but beneath the weak scale is particularly well-motivated, as $U(1)'$ symmetry-breaking and the resulting A' mass may be determined by the same physics that generates the W and Z masses [41]. The best candidate for the origin of the weak scale is low-energy supersymmetry. In this case, the A' can naturally acquire mass suppressed by a loop factor or by $\sqrt{\epsilon}$ compared to the weak scale, leading to MeV to GeV-scale A' masses [13, 35, 41–44]. In supersymmetric models, the gauge kinetic mixing (2) is accompanied by quartic interactions

$$\delta\mathcal{L} \sim \frac{\epsilon_Y}{4} g_Y g_D |\phi_D|^2 |h|^2, \quad (6)$$

between the Standard Model Higgs doublet h and any scalar ϕ_D charged under $U(1)'$, where g_Y and g_D are the gauge couplings of Standard Model hypercharge and the A' coupling to ϕ_D , respectively. Electroweak symmetry breaking gives h a weak-scale vacuum expectation value, so that (6) generates a mass term for ϕ_D . For positively charged ϕ_D , and sufficiently small bare mass, this mass term is negative and triggers $U(1)'$ breaking by the Higgs mechanism. The resulting induced mass for the A' is

$$m_{A'} \sim \sqrt{\epsilon} \sqrt{\frac{g_D g_Y}{g_2^2}} m_W \sim \text{MeV–GeV}, \quad (7)$$

where g_2 is Standard Model $SU(2)_L$ gauge coupling and m_W is the W-boson mass. The resulting mass is precisely in the 50 – 1000 MeV range targeted by this experiment. Given our ϵ sensitivity, we expect to probe the portion of this parameter space with small g_D . For example, for $g_D \sim 0.04$ and $\epsilon \sim 5 \times 10^{-4}$ ($\alpha'/\alpha \sim 2.5 \times 10^{-7}$), we have $m_{A'} \sim 400$ MeV, which can definitively be probed by the proposed experiment. Note that the mechanism of $U(1)'$ breaking above does not rely on supersymmetry, as any quartic interaction of the form (6), with arbitrary coupling, can transmit electro-weak masses to the A' . Thus, the mass relation (7) should not be interpreted too literally.

We stress that the mass of the A' breaks any apparent symmetry between it and the photon: though Standard Model particles have induced ϵ -suppressed charges under the A' , any new matter charged under the A' would *not*

have any effective coupling to the photon, and would have gone undetected.

An electron beam scattering on a high- Z target such as Tungsten will produce A' 's through bremsstrahlung reactions with a cross-section

$$\sigma_{A'} \sim 100 \text{ pb} \left(\frac{\epsilon}{10^{-4}} \right)^2 \left(\frac{100 \text{ MeV}}{m_{A'}} \right)^2, \quad (8)$$

several orders of magnitude larger than in colliding electron and hadron beams [7]. The A' can decay to electrons, and is therefore visible as a narrow resonance in the trident e^+e^- mass spectrum.

Such a new gauge boson would constitute the first discovery of a new gauge force since the observation of Z -mediated neutral currents. Besides the obvious physical interest of a fifth force, the A' like the Z could open up a new “sector” of light, weakly coupled particles whose spectrum and properties could be measured in fixed-target experiments and flavor factories. The A' sector would provide a new laboratory for many physical questions, and would be revealing precisely because its interactions with Standard Model particles are so weak. In particular, if nature is approximately supersymmetric near the TeV scale, the mass scale of supersymmetry breaking for the A' sector is naturally suppressed by ϵ times gauge couplings. In this case, supersymmetry could be studied easily in the A' sector, and possibly even discovered there by relatively low-energy experiments before Standard Model superpartners are seen at colliders.

B. Motivation for an A' from Dark Matter

Dark matter interpretations of recent astrophysical and terrestrial anomalies provide an urgent impetus to search for A' 's in the mass range 50 MeV – 1 GeV, with a coupling $\epsilon \sim 10^{-4} - 10^{-2}$.

The concordance model of big bang cosmology — the “Lambda Cold Dark Matter” (Λ CDM) model — explains all observations of the cosmic microwave background, large scale structure formation, and supernovae, see e.g. [45–49]. This model suggests that Standard Model particles make up only about 4% of the energy density in the Universe, while “dark energy” and “dark matter” make up 74% and 22%, respectively, of the Universe’s energy density. The concordance model does not require dark matter to have any new interactions beyond gravity with Standard Model particles. However, an intriguing theoretical observation, dubbed the *WIMP miracle*, suggests that dark matter *does* have new interactions. In particular, if dark matter consists of ~ 100 GeV to 10 TeV particles interacting via the electroweak force (“weakly interacting massive particles” or “WIMPs”), they would automatically have the right relic abundance observed today.

In addition to the WIMP miracle, evidence from cosmic-ray data and the terrestrial direct dark matter detection experiment DAMA/LIBRA strongly suggest that

dark matter interacts with ordinary matter *not* just gravitationally. While the WIMP miracle suggests that dark matter is charged under the Standard Model electroweak force, we will see that *these observations provide impressive evidence for dark matter interacting with ordinary matter through a new force, mediated by a new 50 MeV – 1 GeV mass gauge boson*. In addition to explaining any or all of these observations, dark matter charged under this new force automatically has the correct thermal relic abundance observed today by virtue of its interactions via the new force carrier, reproducing the success of the WIMP dark matter hypothesis.

The satellites PAMELA [50] and Fermi [51], the balloon-borne detector ATIC [52], the ground-based telescope HESS [53, 54], as well as other experiments, observe an excess in the cosmic-ray flux of electrons and/or positrons above backgrounds expected from normal astrophysical processes. If their source is dark matter annihilation or decay, synchrotron radiation from these electrons and positrons could also explain the “WMAP haze” near the Galactic center [55], which consists of an excess seen in the WMAP Cosmic Microwave Background data. In addition, starlight near the Galactic center would inverse Compton scatter off the high energy electrons and positrons and produce an excess in gamma-rays. A detection of a gamma-ray excess towards the Galactic center region in the gamma-ray data obtained with the Fermi satellite was recently reported in [56], and has been dubbed the “Fermi haze”.

Taken together, these observations by several experimental collaborations provide compelling evidence that there is an unexplained excess in cosmic-ray electrons and positrons in our Galaxy. Given the firm evidence for a 22% dark matter content of the Universe, a very natural source of these excesses is dark matter annihilation. However, two features of these observations are incompatible with annihilation of ordinary thermal WIMP dark matter. They instead provide impressive evidence that dark matter is charged under a new $U(1)'$ and annihilating into the A' , which decays directly into electrons and positrons, or into muons that decay into electrons and positrons, see Figure 2 (left) (see e.g. [5, 57–63]). These two features are:

- The annihilation cross-section required to explain the signal is 50-1000 times larger than the thermal freeze-out cross-section for an ordinary WIMP that is needed to reproduce the observed dark matter relic density. This can be explained if dark matter interacts with a new long range force mediated by an $\mathcal{O}(\text{GeV})$ mass gauge boson, which allows the dark matter annihilation cross-section ($\langle\sigma v\rangle$) to be enhanced at low dark matter velocities, i.e. $\langle\sigma v\rangle \propto 1/v$. In this case, in the early Universe when the dark matter velocity was high ($\sim 0.3c$), the annihilation cross-section that determines the relic abundance can naturally be the same as that of an ordinary WIMP and reproduce the WIMP miracle. However, in the Milky Way halo now, the

dark matter has a much lower velocity ($v \sim 10^{-3}c$), leading to a large increase in the annihilation cross-section that is required to explain the cosmic-ray data. The enhancement at low velocities through a new long-range force is very well known and called the Sommerfeld effect [64].

- The PAMELA satellite did *not* see an anti-proton excess [65], which strongly suggests that dark matter annihilation is dominantly producing leptons, and not baryons. If dark matter is interacting via a $\mathcal{O}(\text{GeV})$ mass force particle in order to have a large annihilation rate via the Sommerfeld mechanism, then annihilations into the force carrier automatically fail to produce any baryons. Kinematically, the force carriers cannot decay into baryons, and are instead forced to decay into the lighter charged leptons. Thus, annihilation products of dark matter are leptonic in this case.

To explain the additional sources of evidence for a new GeV scale force, we briefly summarize the consequence for dark matter mass spectra that follow from dark matter carrying a charge under a new force. If dark matter is charged under a non-Abelian force that acquires mass, then radiative effects can split all components of the dark matter with size, $\delta \sim \alpha_D \Delta m_{W_D}$, where α_D is the non-Abelian fine structure constant and Δm_{W_D} is the splitting of gauge boson masses [57]. Typically, these splittings are $\Delta m_{W_D} \sim \alpha_D m_{W_D} \sim 1 - 10 \text{ MeV}$ for $m_{W_D} \sim 1 \text{ GeV}$ [57]. Thus, $\delta \sim 100 \text{ keV}$ for $\alpha_D \sim 10^{-2}$. These splittings are completely analogous to the splittings that arise between the π^\pm and π^0 from Standard Model $SU(2)$ breaking. If instead a non-Abelian force confines at a scale $\Lambda_D \sim \text{GeV}$, then a heavy-flavor meson can be cosmologically long-lived and thus a dark matter candidate [66]. Hyperfine interactions can naturally induce $\sim 100 \text{ keV}$ splittings of the dark matter particles in this case. We emphasize that the GeV scale force carrier particles mediate quantum corrections that generate the 100 keV and 1-10 MeV splittings of dark matter states [57, 66–68].

When mass splittings arise, A' mediated interactions of dark matter with ordinary matter as well as dark matter self-interactions are dominated by inelastic collisions [57]. The direct dark matter detection experiment DAMA/LIBRA as well as the INTEGRAL telescope provide intriguing evidence for such interactions. The DAMA/NaI [69] and DAMA/LIBRA [70] experiments have reported an annual modulation signal over nearly eleven years of operation with more than 8σ significance. Modulation is expected because the Earth’s velocity with respect to the dark matter halo varies as the Earth moves around the sun, and the phase of the observed modulation is consistent with this origin. A simple hypothesis that explains the spectrum and magnitude of the signal, and reconciles it with the null results of other experiments, is that dark matter-nucleus scatter-

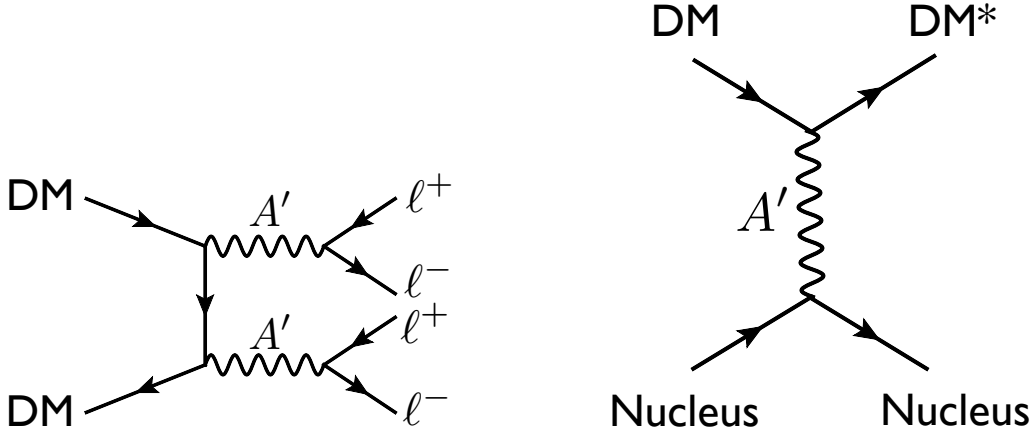


FIG. 2: **Left:** Dark matter annihilation into the dark photon A' , which decays into charged leptons such as electrons and/or muons, can explain the cosmic-ray electron and/or positron excesses seen by PAMELA, Fermi, ATIC, HESS, and other experiments. **Right:** Dark matter scattering into an excited state off nuclei through A' exchange in direct dark matter detection experiments can explain the annual modulation signal observed by DAMA/LIBRA, and the null results of other direct detection experiments.

ing is dominated by an inelastic process,

$$\chi N \rightarrow \chi^* N, \quad (9)$$

in which the dark matter χ scatters off a nucleus N into an excited state χ^* with mass splitting $\delta \approx 100$ keV [67]. The kinematics of these reactions is also remarkably consistent with all the distinctive properties of the nuclear recoil spectrum reported by DAMA/LIBRA. In addition, the INTEGRAL telescope [71] has reported a 511keV photon signal near the galactic center, indicating a new source of ~ 1 -10 MeV electrons and positrons. This excess could be explained by collisions of $\mathcal{O}(100 \text{ GeV}-1 \text{ TeV})$ mass dark matter into $\mathcal{O}(\text{MeV})$ excited states in the galaxy [72] — dark matter excited by scattering decays back to the ground state by emitting a soft e^+e^- pair. The 511keV excess then arises from the subsequent annihilation of the produced positrons.

The existence of an A' may also help explain various other particle physics anomalies [27] such as the anomalous magnetic moment of the muon $((g-2)_\mu)$ [73] and the HyperCP anomaly [74].

While these experimental hints provide an urgent motivation to look for an A' , it is important to emphasize the value of these searches in general. There has never been a systematic search for new GeV-scale force carriers that are weakly coupled to Standard Model particles. Nothing forbids their existence, and their discovery would have profound implications for our understanding of nature. A relatively simple experiment using the facilities available at, for example, Jefferson Laboratory and Mainz will probe a large and interesting range of A' masses and couplings.

C. Current Limits on Light $U(1)$ Gauge Bosons

Constraints on new A' 's that decay to e^+e^- and the search reach of an experiment using the spectrometers of Hall A at Jefferson Laboratory are summarized in Figure 1. Shown are constraints from electron and muon anomalous magnetic moment measurements, a_e and a_μ [27], the BaBar search for $\Upsilon(3S) \rightarrow \gamma A' \rightarrow \gamma \mu^+ \mu^-$, and three beam dump experiments, E137, E141, and E774 [3]. The constraints from a_μ and the BaBar search assume that the A' couples to muons — this is the case, for example, if it mixes with the photon. If it only couples to electrons, then the constraints on α'/α and $m_{A'}$ in the region to which the proposed experiment is sensitive are weaker than $\alpha'/\alpha \lesssim 10^{-4}$.

We refer the reader to [3, 27] for details on existing constraints. Here, we briefly review the constraint on $e^+e^- \rightarrow \gamma A' \rightarrow \gamma \mu^+ \mu^-$ derived from the BaBar search [75]. If the A' couples to both electrons and muons, this is the most relevant constraint in the region probed by the proposed experiment. The analysis of [75] was in fact a search for $\Upsilon(3S)$ decays into a pseudoscalar a , $\Upsilon(3S) \rightarrow \gamma a \rightarrow \gamma \mu^+ \mu^-$, but can be interpreted as a limit on A' production because the final states are identical. Using $\mathcal{L}_{\text{int}} \sim 30 \text{ fb}^{-1}$ of data containing $\sim 122 \times 10^6$ $\Upsilon(3S)$ events, a 90% C.L. upper limit of roughly $(1-4) \times 10^{-6}$ on the $\gamma \mu^+ \mu^-$ branching fraction was found for $m_{A'} \sim 2m_\mu - 1 \text{ GeV}$. This search would thus be sensitive to about $\sim 100-500$ events with $e^+e^- \rightarrow \gamma A' \rightarrow \gamma \mu^+ \mu^-$. Requiring that $\sigma(e^+e^- \rightarrow \gamma A') \times BR(A' \rightarrow \mu^+ \mu^-) \times \mathcal{L}_{\text{int}} \lesssim 500$, where $BR(A' \rightarrow \mu^+ \mu^-) = 1/(2 + R(m_{A'}))$ for $m_{A'} > 2m_\mu$ with $R = \frac{\sigma(e^+e^- \rightarrow \text{hadrons}; E=m_{A'})}{\sigma(e^+e^- \rightarrow \mu^+ \mu^-; E=m_{A'})}$, and rescaling the resulting

constraint to represent a 95% C.L. upper bound, we find the constraint depicted in Figure 1. For $m_{A'} \gtrsim 2m_\mu$, this requires $\alpha'/\alpha \gtrsim 10^{-5}$, while the constraint weakens at higher masses, especially near the ρ -resonance. See [87] for a comparison of our sensitivity estimate to those previously published.

We caution that systematic uncertainties in the A' limit beyond those quoted in [75] may slightly weaken the resulting limit, which should therefore be taken as a rough approximation unless further analysis is done. First, A' production in B-factories is more forward-peaked than the $\Upsilon(3S)$ decay mode considered in [75], so that the signal acceptance is more uncertain. In addition, background distributions in [75] are derived from smooth polynomial fits to data collected on the $\Upsilon(4S)$ resonance, which is assumed to contain no signal. This assumption is not correct for A' production, though the resulting systematic effects are expected to be small.

D. Sensitivity of Potential Searches using Existing Data

Several past and current experiments have data that could be used to significantly improve current limits on α'/α , as discussed in [4, 8, 27]. Here, we estimate the potential sensitivity of searches in three channels ($\pi^0 \rightarrow \gamma A' \rightarrow \gamma e^+ e^-$, $\phi \rightarrow \eta A' \rightarrow \eta e^+ e^-$, and $e^+ e^- \rightarrow \gamma A' \rightarrow \gamma \mu^+ \mu^-$), considering only the statistical uncertainties and irreducible backgrounds. These are likely overestimates, as we are unable to include either systematic uncertainties or significant instrumental backgrounds such as photon conversion in the detector volume.

BaBar, BELLE, and KTeV (E799-II) have produced and detected large numbers of neutral pions, of order 10^{10} , of which roughly 1% decay in the Dalitz mode $\pi^0 \rightarrow e^+ e^- \gamma$. These experiments can search for the decay $\pi^0 \rightarrow \gamma A'$ induced by A' -photon kinetic mixing, which would appear as a narrow resonance over the continuum Dalitz decay background. KTeV has the largest π^0 sample, and its $e^+ e^-$ mass resolution can be approximated from the reported measurement of the $\pi^0 \rightarrow e^+ e^-$ branching fraction [76] to be roughly 2 MeV. This paper also reports the measured mass distribution of Dalitz decays above 70 MeV, from which we estimate potential sensitivity to α'/α as small as 5×10^{-7} for $70 < m(e^+ e^-) \lesssim 100$ MeV, as shown by the orange shaded region in Figure 3.

Similarly, KLOE can search for the decay $\phi \rightarrow \eta A'$, likewise induced by A' kinetic mixing with the photon, in a sample of 10^{10} ϕ 's. An analysis of this data is ongoing [77]. We have taken the blue dashed curve in Figure 3 from [4], which assumes that mass resolution σ_m is dominated by KLOE's 0.4% momentum resolution. We have adjusted the contours from [4] to determine a 2σ contour and enlarged the bin width used to determine signal significance from σ_m in [4] to $2.5\sigma_m$. Above the

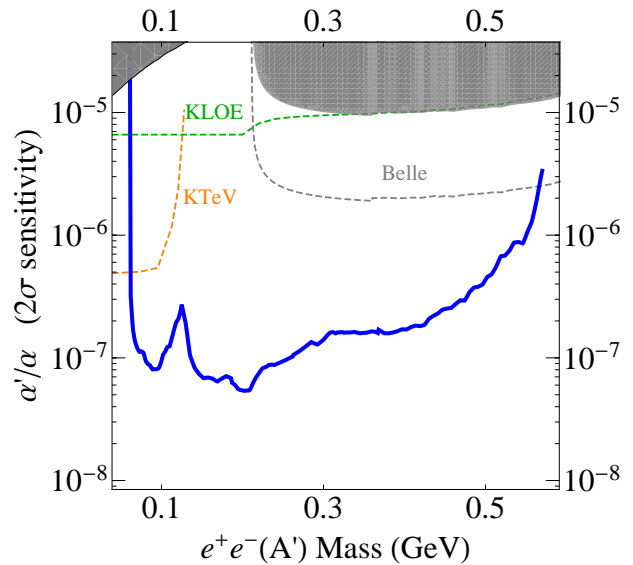


FIG. 3: Anticipated 2σ sensitivity in $\alpha'/\alpha = \epsilon^2$ for the A' experiment (APEX) at Hall A in JLab (thick blue line), compared with current limits and estimated potential 2σ sensitivity for A' searches in existing data (dashed lines), assuming optimal sensitivity as described in the text. From left to right: KTeV $\pi^0 \rightarrow \gamma A' \rightarrow \gamma e^+ e^-$ (orange dashed curve), KLOE $\phi \rightarrow \eta A' \rightarrow \eta e^+ e^-$ (green dashed curve) and Belle $e^+ e^- \rightarrow \gamma A' \rightarrow \gamma \mu^+ \mu^-$ (gray dashed curve). Existing constraints are as in Figure 1.

muon threshold, ϕ decays are not competitive with B -factory continuum production.

In addition, BaBar and Belle can search for the continuum production mode $e^+ e^- \rightarrow \gamma A' \rightarrow \gamma \mu^+ \mu^-$ in their full datasets. For example, an analysis of the Belle $\Upsilon(4S)$ data set would increase statistics by a factor of ~ 24 relative to the BaBar $\Upsilon(3S)$ search that we have interpreted as a limit above. We have derived the expected sensitivity (shown as a black dashed line in Figure 3) simply by scaling the $\Upsilon(3S)$ estimated reach by $\sqrt{24}$. These searches have not been extended below the muon threshold because of large conversion backgrounds.

III. A' PRODUCTION IN FIXED TARGET INTERACTIONS

A' particles are generated in electron collisions on a fixed target by a process analogous to ordinary photon bremsstrahlung, see Figure 4. This can be reliably estimated in the Weizsäcker-Williams approximation (see [3, 78–80]). When the incoming electron has energy E_0 , the differential cross-section to produce an A' of mass

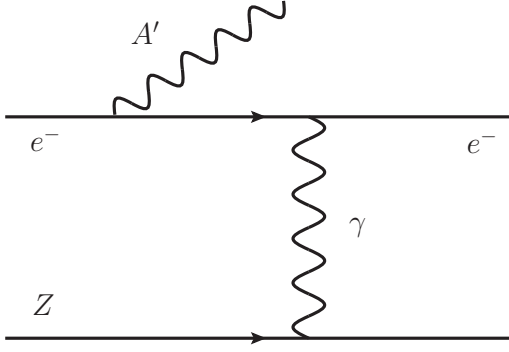


FIG. 4: A' production by bremsstrahlung off an incoming electron scattering off protons in a target with atomic number Z .

$m_{A'}$ with energy $E_{A'} \equiv xE_0$ is

$$\frac{d\sigma}{dx d\cos\theta_{A'}} \approx \frac{8Z^2\alpha^3\epsilon^2 E_0^2 x}{U^2} \tilde{\chi} \times \left[\left(1 - x + \frac{x^2}{2}\right) - \frac{x(1-x)m_{A'}^2 (E_0^2 x \theta_{A'}^2)}{U^2} \right] \quad (10)$$

where Z is the atomic number of the target atoms, $\alpha \simeq 1/137$, $\theta_{A'}$ is the angle in the lab frame between the emitted A' and the incoming electron,

$$U(x, \theta_{A'}) = E_0^2 x \theta_{A'}^2 + m_{A'}^2 \frac{1-x}{x} + m_e^2 x \quad (11)$$

is the virtuality of the intermediate electron in initial-state bremsstrahlung, and $\tilde{\chi} \sim 0.1 - 10$ is the Weizsäcker-Williams effective photon flux, with an overall factor of Z^2 removed. The form of $\tilde{\chi}$ and its dependence on the A' mass, beam energy, and target nucleus are discussed in Appendix A. The above results are valid for

$$m_e \ll m_{A'} \ll E_0, \quad x \theta_{A'}^2 \ll 1. \quad (12)$$

For $m_{A'} \gg m_e$, the angular integration gives

$$\frac{d\sigma}{dx} \approx \frac{8Z^2\alpha^3\epsilon^2 x}{m_{A'}^2} \left(1 + \frac{x^2}{3(1-x)}\right) \tilde{\chi}. \quad (13)$$

The rate and kinematics of A' radiation differ from massless bremsstrahlung in several important ways:

Rate: The total A' production rate is controlled by $\frac{\alpha^3\epsilon^2}{m_{A'}^2}$. Therefore, it is suppressed relative to photon bremsstrahlung by $\sim \epsilon^2 \frac{m_e^2}{m_{A'}^2}$. Additional suppression from small $\tilde{\chi}$ occurs for large $m_{A'}$ or small E_0 .

Angle: A' emission is dominated at angles $\theta_{A'}$ such that $U(x, \theta_{A'}) \lesssim 2U(x, 0)$ (beyond this point, wide-angle emission falls as $1/\theta_{A'}^4$). For x near its median value, the cutoff emission angle is

$$\theta_{A' \text{ max}} \sim \max \left(\frac{\sqrt{m_{A'} m_e}}{E_0}, \frac{m_{A'}^{3/2}}{E_0^{3/2}} \right), \quad (14)$$

which is parametrically smaller than the opening angle of the A' decay products, $\sim m_{A'}/E_0$. Although this opening angle is small, the backgrounds mimicking the signal (discussed in §VI) dominate at even smaller angles.

Energy: A' bremsstrahlung is sharply peaked at $x \approx 1$, where $U(x, 0)$ is minimized. When an A' is produced, it carries nearly the entire beam energy — in fact the median value of $(1-x)$ is $\sim \max \left(\frac{m_e}{m_{A'}}, \frac{m_{A'}}{E_0} \right)$.

The latter two properties are quite important in improving signal significance, and are discussed further in §VI.

Assuming the A' decays into Standard Model particles rather than exotics, its boosted lifetime is

$$\ell_0 \equiv \gamma c \tau \simeq \frac{3E_{A'}}{N_{\text{eff}} m_{A'}^2 \alpha \epsilon^2} \simeq \frac{0.8 \text{ cm}}{N_{\text{eff}}} \left(\frac{E_0}{10 \text{ GeV}} \right) \left(\frac{10^{-4}}{\epsilon} \right)^2 \left(\frac{100 \text{ MeV}}{m_{A'}} \right)^2, \quad (15)$$

where we have neglected phase-space corrections, and N_{eff} counts the number of available decay products. If the A' couples only to electrons, $N_{\text{eff}} = 1$. If the A' mixes kinetically with the photon, then $N_{\text{eff}} = 1$ for $m_{A'} < 2m_\mu$ when only $A' \rightarrow e^+e^-$ decays are possible, and $2 + R(m_{A'})$ for $m_{A'} \geq 2m_\mu$, where $R = \frac{\sigma(e^+e^- \rightarrow \text{hadrons}; E=m_{A'})}{\sigma(e^+e^- \rightarrow \mu^+\mu^-; E=m_{A'})}$ [81]. For the ranges of ϵ and $m_{A'}$ probed by this experiment, the mean decay length $\ell_0 \lesssim 250 \mu\text{m}$ is not significant, but the ability to cleanly reconstruct vertices displaced forward by a few cm would open up sensitivity to considerably lower values of ϵ .

The total number of A' produced when N_e electrons scatter in a target of $T \ll 1$ radiation lengths is

$$N \sim N_e \frac{N_0 X_0}{A} T \frac{Z^2 \alpha^3 \epsilon^2}{m_{A'}^2} \tilde{\chi} \sim N_e C T \epsilon^2 \frac{m_e^2}{m_{A'}^2}, \quad (16)$$

where X_0 is the radiation length of the target in g/cm^2 , $N_0 \simeq 6 \times 10^{23} \text{ mole}^{-1}$ is Avogadro's number, and A is the target atomic mass in g/mole . The numerical factor $C \approx 5$ is logarithmically dependent on the choice of nucleus (at least in the range of masses where the form-factor is only slowly varying) and on $m_{A'}$, because, roughly, $X_0 \propto \frac{A}{Z^2}$ (see [3] and [81]). For a Coulomb of incident electrons, the total number of A' 's produced is given by

$$\frac{N}{C} \sim 10^6 \tilde{\chi} \left(\frac{T}{0.1} \right) \left(\frac{\epsilon}{10^{-4}} \right)^2 \left(\frac{100 \text{ MeV}}{m_{A'}} \right)^2. \quad (17)$$

The spectrometer efficiency can be estimated from Monte Carlo simulation of the signal, discussed in §V. It is quite low in APEX, but of course depends on the precise spectrometer settings. For example, for $m_{A'} = 200 \text{ MeV}$, $E_0 = 3.056 \text{ GeV}$, an angular acceptance window of $\theta_x = 0.055 - 0.102 \text{ rad}$ and $|\theta_y| \leq 0.047 \text{ rad}$ (corresponding to an HRS central angle of 4.5°) and a momentum acceptance of $E = 1.452 - 1.573 \text{ GeV}$ for both the

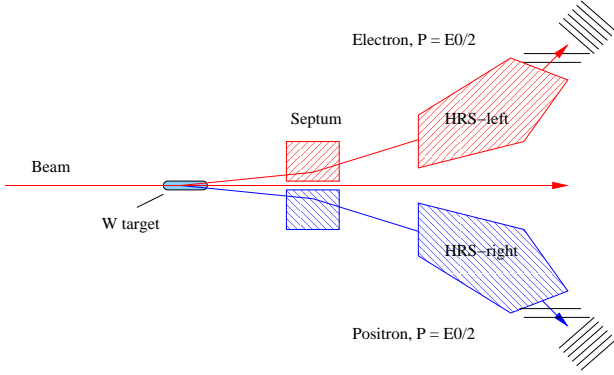


FIG. 5: The layout of the experimental setup — see text for details.

positron and one of the electrons, gives a spectrometer efficiency of $\sim 0.14\%$.

IV. EXPERIMENTAL SETUP

In this section, we describe the experimental setup of the APEX experiment in JLab Hall A. Many of these features are also readily adaptable to other experimental facilities.

The APEX experiment will measure the invariant mass spectrum of e^+e^- pairs produced by an incident beam of electrons on a tungsten target. The experiment uses the two high-resolution spectrometers (HRS) [82] available in Hall A at JLab (see Table I for design specifications), together with a septum magnet constructed for the PREX experiment [26], see Figure 5. The physical angle of the HRS with respect to the beam line does not go below $\sim 12^\circ$, but the septum allows smaller angles to be probed down to $\sim 4^\circ - 5^\circ$ by bending charged tracks outward. The detector package in each HRS available in JLab Hall A includes two vertical drift chambers (VDC), the single photo-multiplier tube (PMT) trigger scintillator counter (“S0 counter”), the Gas Cherenkov counter, the segmented high-resolution scintillator hodoscope, and the double-layer lead-glass shower counter.

The electron beam has a current of $80 \mu A$ (corresponding to $\sim 7 C$ on target per day!), and will be incident on a solid target located on a target ladder in a standard scattering chamber. The target will be made of tungsten wires strung together in a horizontal plane orthogonal to the beam direction. The target plane will be mounted at an angle of about 10 mrad with respect to the horizontal plane. The beam will be rastered by $\pm 0.25 \text{ mm}$ in the horizontal and $\pm 2.5 \text{ mm}$ in the vertical direction to avoid melting the target.

The electron will be detected in the the right HRS (HRS-R) and the positron will be detected in the left HRS (HRS-L). The trigger will be formed by a coincidence of two signals from the S0 counters of the two arms

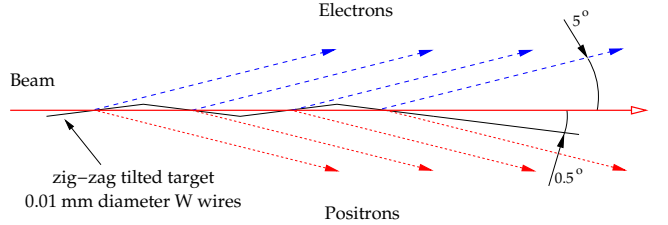


FIG. 6: The top view of the tilted target. The beam is rastered over an area $0.5 \times 5 \text{ mm}^2$ (the latter is in the vertical direction). The beam intersects the target in four areas spread over almost 500 mm . Pair components will be detected by two HRS spectrometers at a central angle of $\pm 5^\circ$. Each zig-zag of the target plane is tilted with respect to the beam by 0.5° and consists of a plane of parallel wires perpendicular to the beam. This reduces the multiple scattering of the outgoing e^+e^- pair (produced in a prompt A' decay), as described in the text.

and a coincidence of the signal in the S0 counters with a signal from the Gas Cherenkov counter of the HRS-L (positive polarity arm). A timing window of 20 ns will be used for the first coincidence and 40 ns for the second coincidence. The resulting signal will be used as a primary trigger of data acquisition (DAQ). An additional logic will be arranged with a 100 ns wide coincidence window between signals from the S0 counters. This second type of trigger will be prescaled by a factor 20 for DAQ, and is used to evaluate the performance of the primary trigger. Most of the DAQ rate will come from events with a coincident electron and positron within a 20 ns time interval.

Note that since we want to search for a narrow peak in the invariant mass spectrum of e^+e^- pairs, which requires a high level of statistical precision, it is especially important to have a very small level of systematics and a smooth invariant mass acceptance. In [1], we show that APEX has these properties.

A. The long tilted target

The experiment will utilize the standard Hall A scattering chamber as it is used by the PREX experiment, with a target consisting of a 50-cm -long tilted wire mesh plane. The concept of the target is presented in Figures 6 and 7. The wires comprising each plane are perpendicular to the beam-line. The tilt angle of 10 mrad is sufficient to ensure stability of the beam-target geometry, and at the same time such a tilt angle is 10 times smaller than the central angle to the HRS, which results in a reduction of the path length traversed by the produced e^+e^- pairs. The wires comprising of each zig-zag plane are spaced so that outgoing e^+e^- pairs coming from prompt A' decays inside a wire only travel through a single wire (for some configurations, the outgoing e^+e^- pair may not have to traverse any wire if the A' does not decay inside

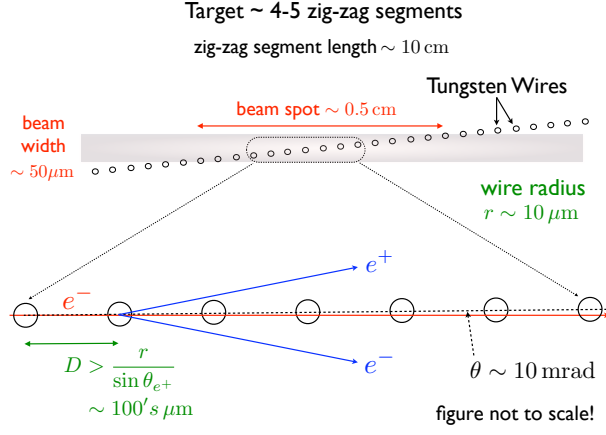


FIG. 7: A schematic close-up view of the target. The figure is not to scale. The target consists of 4–5 zig-zag planes, with each plane consisting of tungsten wires strung together. Each zig-zag plane is ~ 10 cm long, and lies at an angle of ~ 10 mrad with respect to the beam line. The tungsten wires have a radius of $\sim 10\mu\text{m}$ and are spaced at a distance of ~ 100 's μm . While each beam electron can traverse up to ~ 10 wires, the production and prompt decay of an A' in a wire produces e^+e^- pairs that have an angle of $\sim m_{A'}/E_{\text{beam}}$, large enough for them to miss the next wire — this greatly reduces the multiple scattering, and is the reason for not using a target foil. The beam width is $\sim 50\mu\text{m}$, which translates into a $\sim 0.5\text{cm}$ large beam spot along the target plane. The vertical rastering of the beam of $\sim 0.5\text{mm}$ moves the beam spot $\sim 5\text{cm}$ back-and-forth along the target plane — this helps to prevent the beam from melting the target.

a wire). For wire thickness of $\sim 10^{-3}$ radiation lengths, this considerably reduces the multiple scattering in the target versus that in a true foil and leads to a much better mass resolution. The maximum number of wires that a beam electron can pass through per plane is ~ 10 in the configuration illustrated in Figure 6 or Figure 7 assuming $10\mu\text{m}$ diameter tungsten wires. Wires as thick as $15\mu\text{m}$ can be used without significantly compromising mass resolution.

The plane of the target wire mesh will be vertical. The mesh plane will have 4–5 zig-zags, each with length 5–10 cm, which result in multiple intersection points allowing an extra factor of 4–5 for rejection of accidental tracks in offline analysis. (Figure 6 illustrates a target with 4 zig-zags.)

The central angle of the spectrometer varies with the position of the target. In this experiment, such a variation is very useful because it extends the range of invariant mass covered with one setting of the spectrometers. For several settings suggested in our run plan, only two planes of wire mesh are needed, one at the front and one at the back of the acceptance region.

There are two considerations to take into account when selecting the material. The first consideration is to achieve the highest possible ratio of signal to background, while keeping the background rate low enough so as not

TABLE I: Main design characteristics of the Hall A High Resolution Spectrometers at nominal target position (see [82] for more details). The resolution values are for the full-width at half-maximum. These parameters correspond to a point target and do not include the effects of multiple scattering in the target and windows. In the calculation of the invariant mass resolution the effect of multiple scattering in the target was taken into account. The vacuum coupling of the scattering chamber and the spectrometer allows one to avoid using windows.

Configuration	QQD _n Q Vertical bend
Bending angle	45°
Optical length	23.4 m
Momentum range	0.3 - 4.0 GeV/c
Momentum acceptance	$-4.5\% < \delta p/p < +4.5\%$
Momentum resolution	1×10^{-4}
Dispersion at the focus (D)	12.4 m
Radial linear magnification (M)	-2.5
D/M	5.0
Angular range HRS-L	12.5° - 150°
HRS-R	12.5° - 130°
Angular acceptance: Horizontal	± 30 mrad
Vertical	± 60 mrad
Angular resolution : Horizontal	0.5 mrad
Vertical	1.0 mrad
Solid angle at $\delta p/p = 0, y_0 = 0$	6 msr
Transverse length acceptance	± 5 cm
Transverse position resolution	1 mm

to overwhelm the triggering and DAQ system. The second is whether a thin foil or a thin wire of a particular material is available. Large backgrounds come from pions produced in photo-production from nucleons, and from electrons produced in the radiative tail of electron-proton elastic scattering. These backgrounds do not mimic the signal, but if their rate is too large, they can overwhelm the DAQ system. These considerations favor the use of a tungsten target, with a total thickness between 0.5% and 10% radiation length, with thicker targets used in higher-energy runs. Reduction of the thickness at low energies is required to limit the rate in the electron spectrometer and also minimizes the multiple-scattering contribution to the pair mass resolution.

The heat load of the target is also an important consideration. This is mitigated by rastering the beam and using materials like tantalum or tungsten. The tilted target cools from a large area; for example, with the raster size 0.5×5 mm and proposed geometry (Figure 6), the cooling area is 20 cm^2 . For the parameters of APEX (an electron beam of $80\mu\text{A}$ on a 10% X_0 tungsten target) the head load is about 140 W (or 7 W/cm^2), which results in the equilibrium target temperature of 1000°K . Experimental study has demonstrated that 1 kW/cm^2 is

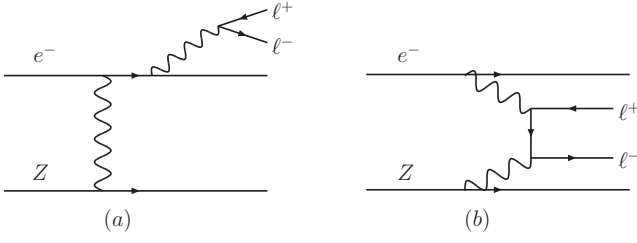


FIG. 8: Sample diagrams of (a) radiative trident (γ^*) and (b) Bethe-Heitler trident reactions that comprise the primary QED background to $A' \rightarrow \ell^+ \ell^-$ search channels.

a safe level for a tungsten foil target [83], so we expect that the wire mesh target will perform quite well.

V. SIGNAL AND TRIDENT KINEMATICS

The stark kinematic differences between QED trident backgrounds and the A' signal are the primary considerations in determining the momentum settings of the spectrometers. As we will show in §VI, QED tridents dominate the final event sample after offline rejection of accidentals, so we consider their properties in some detail here.

The irreducible background rates are given by the diagrams shown in Figure 8. These trident events can be usefully separated into “radiative” diagrams (Figure 8(a)), and “Bethe-Heitler” diagrams (Figure 8(b)), that are separately gauge-invariant.

We have simulated the production of these continuum trident background events in QED using the nuclear elastic and inelastic form-factors in [78]. The simulation is done using MadGraph and MadEvent [84] to compute the matrix elements for $e^- Z \rightarrow e^- (e^+ e^-) Z$ exactly, but neglecting the effect of nuclear excitations on the kinematics in inelastic processes. The MadEvent code was modified to properly account for the masses of the incoming nucleus and electron in event kinematics, and the nucleus is assumed to couple with a form-factor G_2 defined in Appendix A.

The continuum trident background was simulated including the full interference effects between the diagrams in Figure 8. In addition, a “reduced-interference” approximation simplifies the analysis and is much less computationally intensive. In this approximation, we treat the recoiling e^- and the e^- from the produced pair as distinguishable. Furthermore, we separate trident processes into the radiative diagrams (Figure 8(a)) and the Bethe-Heitler diagrams (Figure 8(b)), and we calculate the cross-section for both of these diagrams separately. This approximation under-estimates the background rates by a factor of about 2–3 in the range of A' masses and beam energies considered in this paper and [1]. For the reach analysis discussed below, we have used differential distributions computed in the “reduced-interference” approx-

imation, then rescaled to the cross-section for the full-interference process.

The contribution from the radiative diagrams (Figure 8(a)) alone is also useful as a guide to the behavior of A' signals at various masses. Indeed, the kinematics of the A' signal events is identical to the distribution of radiative trident events restricted in an invariant mass window near the A' mass. Moreover, the rate of the A' signal is simply related to the radiative trident cross-section within the spectrometer acceptance and a mass window of width δm by [3]

$$\frac{d\sigma(e^- Z \rightarrow e^- Z(A' \rightarrow \ell^+ \ell^-))}{d\sigma(e^- Z \rightarrow e^- Z(\gamma^* \rightarrow \ell^+ \ell^-))} = \left(\frac{3\pi\epsilon^2}{2N_{\text{eff}}\alpha} \right) \left(\frac{m_{A'}}{\delta m} \right), \quad (18)$$

where N_{eff} counts the number of available decay products and is defined below equation (15). This exact analytic formula was also checked with a MC simulation of both the A' signal and the radiative tridents background restricted to a small mass window δm , and we find nearly perfect agreement. Thus, the radiative subsample can be used to analyze the signal, which simplifies the analysis considerably.

It is instructive to compare kinematic features of the radiative and Bethe-Heitler distributions, as the most sensitive experiment maximizes acceptance of radiative events and rejection of Bethe-Heitler tridents. Although the Bethe-Heitler process has a much larger total cross-sections than either the signal or the radiative trident background, it can be significantly reduced by exploiting its very different kinematics. In particular, the A' carries most of the beam energy (see discussion in §III), while the recoiling electron is very soft and scatters to a wide angle. In contrast, the Bethe-Heitler process is not enhanced at high pair energies. Moreover, Bethe-Heitler processes have a forward singularity that strongly favors asymmetric configurations with one energetic, forward electron or positron and the other constituent of the pair much softer.

These properties are discussed further in the Appendix of [3], and illustrated in Figure 9, which shows a scatter-plot of the energy of the positron and the higher-energy electron for the signal (red crosses) and Bethe-Heitler background (black dots). The signal electron-positron pairs are clearly concentrated near the kinematic limit, $E(e^+) + E(e^-) \approx E_{\text{beam}}$. Background rejection is optimized in symmetric configurations with equal angles for the two spectrometers and momentum acceptance of each spectrometer close to half the beam energy (blue box).

While the signal over background (S/B) can be significantly improved with a judicious choice of kinematic cuts, the final S/B in a small resolution limited mass window is still very low, $\sim 1\%$. A “bump-hunt” for a small signal peak over the continuous background needs to be performed. This requires an excellent mass resolution, which has an important impact on target design and calls for a target that is tilted with respect to the beam line (see Appendix B for a discussion of the mass

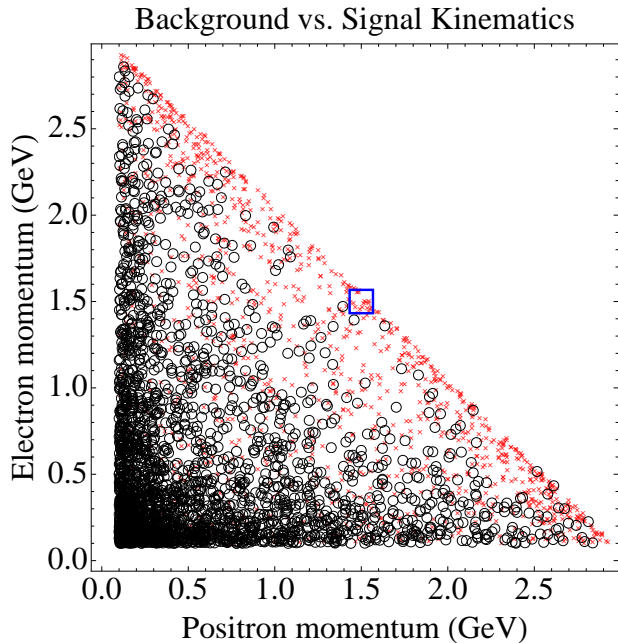


FIG. 9: Positron and electron momenta in A' signal events with $m_{A'} = 200$ MeV (red crosses) and in Bethe-Heitler background events, for a 3 GeV beam energy. Comparably sized signal and Bethe-Heitler samples were used to highlight the kinematics of both; in fact the expected signals are much lower than the Bethe-Heitler process (see Figure 11). The clustering of A' events at high momenta near the kinematic limit and of Bethe-Heitler events along both axes are evident. A spectrometer acceptance window that optimizes signal sensitivity is indicated by the blue box.

resolution).

A. Calculation of the ϵ reach

For all cross sections and rates of reactions described in this paper and [1], Monte Carlo based calculations were performed over a grid of beam energy settings and central spectrometer angular settings. Interpolation was used to extend this grid continuously to intermediate beam energies and angles — all rates exhibited expected power law behavior, thereby providing confidence in the reliability of an interpolation. Additional cross checks at specific points were performed to test the accuracy of our interpolation, which was generally better than $\sim 5\%$.

In order to calculate the α'/α reach for a particular choice of target nucleus, spectrometer angular setting, profile of wire mesh target, and momentum bite, the following procedure is performed:

- Monte Carlo events are simulated for the Bethe-Heitler, radiative tridents, and the continuum trident background including the full interference effects between the diagrams. The latter background is computationally intensive, and only a

small statistics sample is generated, sufficient to obtain the cross-section from MadEvent.

- The cross-section ratio of the full continuum background (with interference effects) to the sum of the Bethe-Heitler and radiative tridents is calculated, and represents a multiplicative factor by which the latter must be multiplied to get the background cross-section.
- The rates of all reactions impinging the spectrometer acceptance were calculated by integrating over a chosen target profile, which usually extended from 4.5 to 5.5 degrees. For Bethe-Heitler, radiative tridents, and the continuum trident background, the calculation of the rate was performed as a function of the invariant mass of the e^+e^- pairs.
- Using the expressions in Appendix B, we calculated the mass resolution δ_m . We then tiled the acceptance region with bins of size $2.5 \times \delta_m$ in invariant mass.
- As a function of α'/α , the total number of signal (S) and background (B) events was calculated with the help of (18) for each bin.
- We then set $S/\sqrt{B} = 2$, and solved for α'/α .

This procedure was used to calculate the reach in the α'/α and $m_{A'}$ parameter space shown in §VII. Further improvements may be obtained by more sophisticated analysis cuts such as the use of matrix element methods (see e.g. [12]).

VI. BACKGROUNDS

In this section, we present the results of an analysis of the expected backgrounds for the A' search. Table II summarizes the expected singles rates, trigger rates, and coincidence rates. For more details on how we calculated the background rates we refer the reader to [1].

Important backgrounds come from electron, pion, and positron singles. There are three contributions to the electron singles rate in the HRS at the proposed momentum settings, namely inelastic scattering, radiative elastic electron-nuclei scattering, and radiative quasi-elastic electron-nucleon scattering. Our calculations of the electron, pion, and positron singles rates were checked against measurements made by experiment E03-012 for a 5 GeV electron beam incident on a hydrogen target, at 6° 2-GeV HRS setting. The final values of the electron and pion rates were obtained by means of the “Wiser” code [85]; positron singles rates from trident reactions were calculated using MadGraph and MadEvent [84], described in §V.

Using our calculations of the singles rates, we compute the rate of accidental coincident triggers arising from an e^+ in the HRS-R and an e^- in the HRS-L within the

Settings	A	B	C	D
Beam energy (GeV)	2.302	4.482	1.1	3.3
Central angle	5.0°	5.5°	5.0°	5.0°
Effective angles	(4.5,5.5)	(5.25,6.0)	(4.5,5.5)	(4.5,5.5)
Target T/X_0 (ratio ^a)	4.25% (1:1)	10% (1:1)	0.58% (1:3)	10% (1:1)
Beam current (μA)	80	80	80	80
Central momentum (GeV)	1.145	2.230	0.545	1.634
Singles (negative polarity)				
e^- (MHz)	4.5	0.7	6.	2.9
π^- (kHz)	640.	2200	36.	2500.
Singles (positive polarity)				
$\pi^+ + p$ (kHz)	640.	2200	36.	2500.
e^+ (kHz)	31.	3.6	24.	23.
Trigger/DAQ:				
Trigger ^b (kHz)	4.	0.4	3.2	3.4
Signal to background:				
Trident (Hz)	610	70	350	530
Two-step (Hz)	35	15	5	75
Background ^c (Hz)	70	1.3	70	35

^a The listed total target thickness is split between two sets of wire mesh planes, located at different z to produce the two indicated effective angles. The numbers in parentheses denote the ratio of target thickness at the larger effective angle to that at the smaller effective angle.

^b Trigger: Coincidence with 20 ns time window between S0-N (assuming pions are rejected by a factor of 100) and S0-P signals.

^c Dominated by e^+e^- accidental rate. We assume pion rejection by a factor of 10^4 in offline cuts, a 2 ns time window and additional factor of 4 rejection of accidentals from the target vertex. Further rejection using kinematics is expected, but not included in the table.

TABLE II: Expected counting rates for the proposed experiment.

trigger timing windows. These accidental coincidences are a dominant part of the recorded events in APEX, and determine the maximum rate at which potential signal trident events can be recorded. A typical composition of the single rate in the spectrometers is expected to be $e^-/\pi^- \approx 80/20$ in the negative polarity arm and $\pi^+/p/e^+ \approx 80/19/1$ in the positive polarity arm. The fraction of the true coincidence events could be up to 50% for the $e^-\pi^+$ rate within a 2 ns time window, and could be significant for the e^-p events in certain regions of momenta.

Besides the trident events discussed in §V, an additional source of true coincidence events is the “two-step” (incoherent) trident process, in which an electron radiates a real, hard photon in the target that subsequently converts to a high-mass e^+e^- pair. For thin targets, this process is suppressed compared to the trident rate, and so it is sub-dominant for all the settings we consider.

The consideration of these rates determine trigger rates and upper bounds on offline accidental rates shown in Table II.

VII. MEASUREMENTS AND REACH IN APEX

We consider a twelve-day run in the configuration “B” of Table II and six-day runs in each of the remaining configurations, to search for new resonances in e^+e^- trident spectra from 65 to 550 MeV. For settings “A” and “C”, the target thickness and beam current have been optimized to accumulate the largest possible sample of trident events without saturating the data acquisition system. Settings “B” and “D” are far from data acquisition limits, but we do not use $T/X_0 > 10\%$ to avoid limits on the total radiation produced (this can possibly be side-stepped at other facilities).

The mass range from 65 to 550 MeV is chosen to take advantage of the Hall A HRS spectrometers, as well as for its theoretical interest. Lower masses are more effectively probed by using lower beam energies, improved forward acceptance, and/or vertexing (see also [12]). Settings at higher masses are possible but have significantly reduced sensitivity and are better suited to exploration with higher-acceptance equipment and an experiment optimized to accept muon and pion pairs as well as electrons.

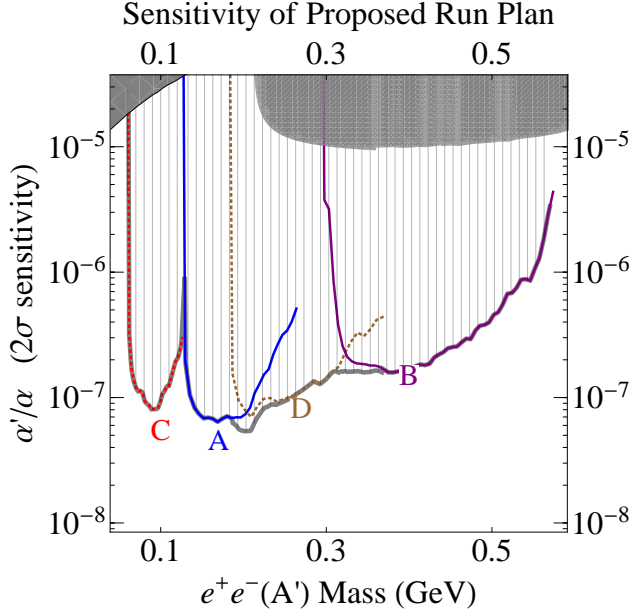


FIG. 10: Anticipated 2σ sensitivity in $\alpha'/\alpha = \epsilon^2$ for APEX [1] for the settings given in Table II (assuming a six-day run in configuration “A”, “C”, and “D” and a twelve-day run in “B”). Existing constraints are shown in the gray shaded regions. The colored curves correspond to the sensitivity in each of the individual energy settings, and the thick gray curve reflects the sensitivity of a combined analysis.

In each setting, the proposed experiment will accumulate between 70 and 300 million trident events. With these statistics, it will be possible to search offline for small resonances comprising a few thousandths of the collected data in a resolution-limited window. This will allow sensitivity to new gauge boson couplings α'/α as low as 10^{-7} over the broad mass range probed by APEX, as summarized in Figure 10. This sensitivity would improve on the cross-section limits from past experiments by a factor of $\sim 10 - 1000$.

As a specific example, we have illustrated the expected sensitivity of setting “A” to A' signals with different ϵ in Figure 11. Each component of the target populates a different invariant mass distribution; for simplicity we consider only the contribution from the front planes of the target, with $\theta_{eff} \approx 5.5^\circ$ (recall that the target is extended along the beam line and consists of 4–5 planes in a zig-zag configuration). The top panel illustrates the absolute size of A' signals at $m_{A'} = 200$ MeV compared to the continuum trident background (gray line) and the size of 2 and 5-sigma statistical fluctuations (blue and green dashed lines), while the bottom panel illustrates how the same signals would appear after subtracting a smooth parameterization of the background. The purple curves in each panel corresponds to an A' signal with $\alpha'/\alpha = 7 \times 10^{-6}$ at 200 MeV, which according to the estimates in §IID would not be seen or excluded at 2σ by a future KLOE search in $\phi \rightarrow \eta A'$. The red curve

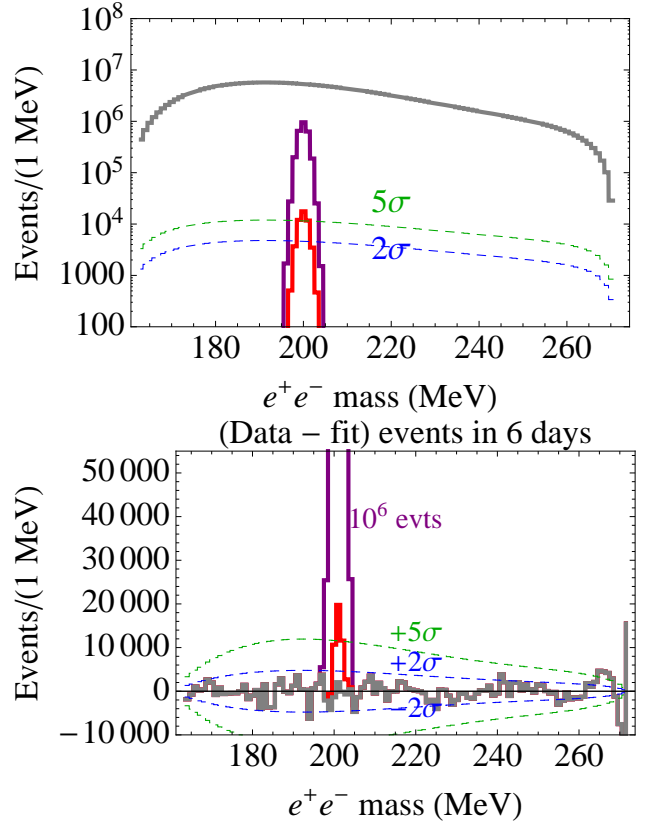


FIG. 11: Comparison of signal rates in six days of running at setting “A” to expected background and statistical sensitivity. **Top:** The resonances in purple and red lines correspond to A' signals at 200 MeV, smeared by a Gaussian to model detector resolution and multiple scattering, with $\alpha'/\alpha = 6.5 \times 10^{-6}$ and 1.3×10^{-7} , respectively. The upper (purple) signal is just beyond the 2σ expected sensitivity of a KLOE analysis, while the lower (red) signal corresponds to the “ 5σ ” sensitivity (not including a trials factor) of this experiment. The gray line is the simulated invariant mass distribution for the continuum trident background, and the blue and green dashed lines reflect the size of 2 and 5σ Poisson fluctuations. **Bottom:** The gray line corresponds to the bin-by-bin differences between pseudodata containing no signal and a smooth fit to this pseudodata. Analogous subtractions when a signal is present are shown in purple and red, with the same α'/α as in the top figure. Again the blue and green dashed lines reflect the size of 2 and 5σ Poisson fluctuations.

has $\alpha'/\alpha = 1.3 \times 10^{-7}$, corresponding to the expected “ 5σ ” sensitivity (not accounting for the trials factor) in APEX.

VIII. CONCLUSIONS

This paper summarized a new experiment (“ A' experiment”, or “APEX”) that has been proposed to the Jefferson Laboratory’s PAC 35 [1]. The experiment proposes to use 30 days of beam to measure the electron-positron

pair mass spectrum and search for new gauge bosons A' in the mass range $65 \text{ MeV} < m_{A'} < 550 \text{ MeV}$ that have weak coupling to the electron. Parametrizing this coupling by the ratio α'/α that controls the A' production cross-section, this experiment would probe α'/α as small as $\sim (6 - 8) \times 10^{-8}$ at masses from 65 to 300 MeV, and $\alpha'/\alpha \sim (2 - 3) \times 10^{-7}$ at masses up to 525 MeV, making it sensitive to production rates 10–1000 times lower than the best current limits set by measurements of the anomalous muon magnetic moment and by direct searches at BaBar. The experiment uses the JLab electron beam in Hall A at energies of about 1, 2, 3, and 4 GeV incident on a long (50 cm) thin tilted tungsten wire mesh target, and both arms of the High Resolution Spectrometer at angles between 5.0° and 5.5° relative to the nominal target position. The experiment can determine the mass of an A' to an accuracy of $\sim 1\text{--}2 \text{ MeV}$.

While this paper was motivated by a specific experimental proposal for JLab Hall A, very similar experiments are possible at other experimental facilities, such as the Mainz Microtron or JLab Hall B. Many of the considerations discussed in this paper are applicable to these other facilities.

Constraints on new vector bosons with mass near 50 MeV – 1 GeV are remarkably weak. However, such light force carriers are well motivated theoretically, and several recent anomalies from terrestrial and satellite experiments suggest that dark matter interacting with Standard Model particles has interactions with new vector bosons in precisely this mass range. The proposed experiment can probe these hypothetical particles with a sensitivity that is unrivaled by any existing or planned experiment.

Acknowledgements

We thank Nima Arkani-Hamed, James Bjorken, Douglas Finkbeiner, Mathew Graham, John Jaros, Takashi Maruyama, Ken Moffeit, Richard Partridge, Michael Peskin, Maxim Pospelov, Allen Odian, Art Snyder, Jay Wacker, and Neal Weiner for many useful discussions and encouragement. We also thank Johan Alwall for answering questions about Madgraph. We especially thank Peter Bosted, Kees de Jager, Doug Higinbotham, John LeRose, and Yi Qiang for their help in preparing the proposal for JLab Hall A. RE and PS are supported by the US DOE under contract number DE-AC02-76SF00515. RE, PS, and NT would like to thank the Kavli Institute for Theoretical Physics in Santa Barbara for hospitality during part of this research. PS and NT also thank the Perimeter Institute for Theoretical Physics for hospitality. We also thank the SLAC National Accelerator Laboratory for providing funding for the “Dark Forces” workshop in September 2009.

Appendix A: Effective Photon Flux, Target Nucleus and Beam-Energy Dependence

In this appendix we summarize the formulas used in Section III for the reduced effective photon flux $\tilde{\chi}$, and highlight its dependence on the A' mass, target nucleus, and beam energy. The effective photon flux χ is obtained as in [78, 79] by integrating electromagnetic form-factors over allowed photon virtualities:

For a general electric form factor $G_2(t)$,

$$\chi \equiv \int_{t_{\min}}^{t_{\max}} dt \frac{t - t_{\min}}{t^2} G_2(t) \quad (\text{A1})$$

(the other form factor, $G_1(t)$, contributes only a negligible amount in all cases of interest). Since we are dominated by a coherent scattering with $G_2 \propto Z^2$, it is useful to define a reduced photon flux,

$$\tilde{\chi} \equiv \chi/Z^2. \quad (\text{A2})$$

The integral in (A1) receives equal contributions at all t , and so is logarithmically sensitive to $t_{\min} = (m_{A'}^2/2E_0)^2$ and $t_{\max} = m_{A'}^2$.

For most energies in question, $G_2(t)$ is dominated by an elastic component

$$G_{2,el}(t) = \left(\frac{a^2 t}{1 + a^2 t} \right)^2 \left(\frac{1}{1 + t/d} \right)^2 Z^2, \quad (\text{A3})$$

where the first term parametrizes electron screening (the elastic atomic form factor) with $a = 111 Z^{-1/3}/m_e$, and the second finite nuclear size (the elastic nuclear form factor) with $d = 0.164 \text{ GeV}^2 A^{-2/3}$. We have multiplied together the simple parametrizations used for each in [78]. The logarithm from integrating (A1) is large for $t_{\min} < d$, which is true for most of the range of interest. However, for heavy A' , the elastic contribution is suppressed and is comparable to an inelastic term,

$$G_{2,in}(t) = \left(\frac{a'^2 t}{1 + a'^2 t} \right)^2 \left(\frac{1 + \frac{t}{4m_p^2}(\mu_p^2 - 1)}{(1 + \frac{t}{0.71 \text{ GeV}^2})^4} \right)^2 Z, \quad (\text{A4})$$

where the first term parametrizes the inelastic atomic form factor and the second the inelastic nuclear form factor, and where $a' = 773 Z^{-2/3}/m_e$, m_p is the proton mass, and $\mu_p = 2.79$ [78]. This expression is valid when $t/4m_p^2$ is small, which is the case for $m_{A'}$ in the range of interest in this paper. At large t the form factors will deviate from these simple parameterizations but can be measured from data. One can show that the contribution from the other inelastic nuclear form factor $G_1(t)$ is negligible.

The resulting reduced form factor $\tilde{\chi}(m^2, E_0) = \chi/Z^2$ are plotted in the left panel of Figure 12 as a function of e^+e^- mass for various electron energies (1, 2, 3, and 4 GeV) incident on a Tungsten target. The relative efficiency of A' production in targets of different compositions but the same thickness in radiation lengths is given

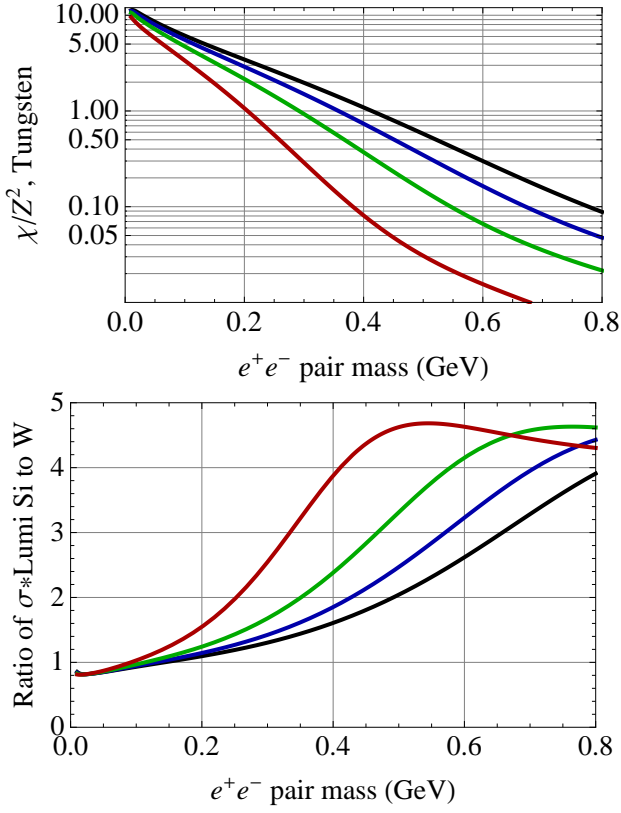


FIG. 12: *Top*: The factor $\tilde{\chi} = \chi/Z^2$ defined in (A2) and (A1) as a function of e^+e^- mass for (bottom to top) 1, 2, 3, and 4 GeV incident electrons on a Tungsten target. *Bottom*: The ratio of (A5) A' production rates per radiation length for Silicon and Tungsten targets, as a function of invariant mass and for beam energies (top to bottom at 0.4 GeV) 1, 2, 3, and 4 GeV incident electrons.

by the ratio

$$R(Z_1, Z_2) = \frac{X_0(Z_1)\chi(Z_1, t)/A(Z_1)}{X_0(Z_2)\chi(Z_2, t)/A(Z_2)}. \quad (\text{A5})$$

For example the ratio $R(\text{Si}, \text{W})$ is shown in the right panel of Figure 12, again as a function of e^+e^- mass for beam energies between 1 and 4 GeV.

Appendix B: Mass resolution

In this appendix, we briefly describe an estimate of the mass resolution of the spectrometer. Since we are looking for a small bump on the invariant mass spectrum distribution, an excellent mass resolution is essential to obtain a good reach in ϵ .

The mass resolution of the spectrometer, δ_m , is roughly given by

$$\left(\frac{\delta_m}{m}\right)^2 = \left(\frac{\delta_p}{p}\right)^2 + 0.5 \times \left(\frac{\delta_\theta}{\theta}\right)^2, \quad (\text{B1})$$

where δ_θ is the angular resolution of the electron or positron, and δ_p/p is the momentum resolution of the HRS, which is always less than 3×10^{-4} (in our estimates for the reach of ϵ , we take $\delta p/p$ to be equal to this upper bound). We have

$$(\delta_\theta)^2 = (\delta_{HRS})^2 + (\delta_\theta^{ms})^2, \quad (\text{B2})$$

where δ_{HRS} is the HRS angular resolution, which is ~ 0.5 mrad in the horizontal direction and ~ 1 mrad in the vertical direction. Moreover, δ_θ^{ms} represents the degradation of the resolution due to multiple Coulomb scattering in the target. It is given by the standard formula [81]

$$\delta_\theta^{ms} = \frac{13.6}{p[\text{MeV}]} \sqrt{\frac{t}{X_0}} \left[1 + 0.038 \ln\left(\frac{t}{X_0}\right) \right], \quad (\text{B3})$$

where t is the thickness in radiation lengths of the material along the path of the particle, X_0 is the radiation length of the target in g/cm^2 , and p is the momentum of particle in MeV.

For the proposed experiment, the thickness of the target along the direction of the beam line varies from $t = 0.003X_0$ to $t = 0.09X_0$. However, in the case of a foil target or a target composed of several thin wires, the distance traversed by trident electron-positron pairs can be significantly smaller because the electron and positron have relatively large angles with respect to the beam line. For a foil, we can take $t \approx \frac{1}{2}t_f/\sin(\theta_p - \theta_f)$, where t_f is the foil thickness and θ_f its angle relative to the beam line. In this case the effective thickness traversed by the beam is $T_0 = t_f/\sin\theta_f$.

In the case of a target composed of multiple wires, as was assumed in determining the experimental sensitivity, the wires can be spaced widely enough that the pair-produced particles need only travel through a single wire. In this case, t is typically the radius of the wire, which for Tungsten wire targets can be as small as $10\mu\text{m}$, or $3 \times 10^{-3}X_0$. In this case, we find that the HRS angular resolution, δ_{HRS} , is comparable to the multiple scattering δ_θ^{ms} in the proposed experiment.

Appendix C: Monte Carlo validation with E04-012 data

In this appendix, we briefly describe a validation of the Monte Carlo (MC) simulation of the signal, Bethe-Heitler and radiative trident backgrounds (shown in Figure 8 and discussed in §V), and the positron singles.

We first discuss a comparison of the MC with previous experimental results from the JLab experiment E04-012 [86]. This experiment consisted of a 5.01 GeV, 14.5 μA electron beam incident on a 1.72% radiation length liquid Hydrogen target. The e^+ singles rate was measured to be ~ 1.1 kHz in a momentum window of $\pm 4\%$ around 1.93 GeV and an angular acceptance of 4.5 msr with an aspect ratio of 2-to-1 centered at an angle of 6° . The e^+e^- coincidence rate was measured at ~ 4 Hz for the same angular

acceptance for both the electron and positron arm, and with a momentum window of $\pm 4\%$ around 1.93 GeV for the positron and $\pm 4\%$ around 1.98 GeV for the electron. We simulated this with MadGraph and MadEvent [84] as described in §V, using a form factor for Hydrogen given in [78]. We find a e^+ singles rate of ~ 965 Hz and an e^+e^- coincidence rate of 3.9 Hz, which agrees with the measured rates to within $\sim 19\%$ and a few percent, re-

spectively.

We have also verified the implementation of form factors in Monte Carlo by simulating photo-production of electrons and muons off Tungsten and Beryllium with MadGraph and MadEvent. The resulting cross-sections agree to within 30% with published computations in the Weizsäcker-Williams approximation [79].

-
- [1] A New Proposal to Jefferson Lab PAC35: Search for a New Vector Boson A' Decaying to e^+e^- , “<http://hallaweb.jlab.org/collab/PAC/PAC35/PR-10-009-Dark-Matter-Search.pdf>.”
 - [2] B. Holdom, *Two $U(1)$ ’s and Epsilon Charge Shifts*, *Phys. Lett.* **B166** (1986) 196.
 - [3] J. D. Bjorken, R. Essig, P. Schuster, and N. Toro, *New Fixed-Target Experiments to Search for Dark Gauge Forces*, *Phys. Rev.* **D80** (2009) 075018, [0906.0580].
 - [4] M. Reece and L.-T. Wang, *Searching for the light dark gauge boson in GeV-scale experiments*, 0904.1743.
 - [5] M. Pospelov and A. Ritz, *Astrophysical Signatures of Secluded Dark Matter*, *Phys. Lett.* **B671** (2009) 391–397, [0810.1502].
 - [6] B. Batell, M. Pospelov, and A. Ritz, *Probing a Secluded $U(1)$ at B-factories*, 0903.0363.
 - [7] R. Essig, P. Schuster, and N. Toro, *Probing Dark Forces and Light Hidden Sectors at Low-Energy $e+e-$ Colliders*, 0903.3941.
 - [8] B. Batell, M. Pospelov, and A. Ritz, *Exploring Portals to a Hidden Sector Through Fixed Targets*, *Phys. Rev.* **D80** (2009) 095024, [0906.5614].
 - [9] F. Bossi, *The role of KLOE and KLOE-2 in the search for a secluded gauge sector*, 0904.3815.
 - [10] P.-f. Yin, J. Liu, and S.-h. Zhu, *Detecting light leptophilic gauge boson at BESIII detector*, 0904.4644.
 - [11] R. Essig, R. Harnik, J. Kaplan, P. Schuster, and N. Toro *to appear*.
 - [12] M. Freytsis, G. Ovanessian, and J. Thaler, *Dark Force Detection in Low Energy $e-p$ Collisions*, 0909.2862.
 - [13] M. Baumgart, C. Cheung, J. T. Ruderman, L.-T. Wang, and I. Yavin, *Non-Abelian Dark Sectors and Their Collider Signatures*, *JHEP* **04** (2009) 014, [0901.0283].
 - [14] C. Cheung, J. T. Ruderman, L.-T. Wang, and I. Yavin, *Lepton Jets in (Supersymmetric) Electroweak Processes*, 0909.0290.
 - [15] **D0** Collaboration, V. M. Abazov *et al.*, *Search for dark photons from supersymmetric hidden valleys*, *Phys. Rev. Lett.* **103** (2009) 081802, [0905.1478].
 - [16] B. Batell, M. Pospelov, and A. Ritz, *Multi-lepton Signatures of a Hidden Sector in Rare B Decays*, 0911.4938.
 - [17] B. Batell, M. Pospelov, A. Ritz, and Y. Shang, *Solar Gamma Rays Powered by Secluded Dark Matter*, 0910.1567.
 - [18] P. Schuster, N. Toro, and I. Yavin, *Terrestrial and Solar Limits on Long-Lived Particles in a Dark Sector*, 0910.1602.
 - [19] P. Schuster, N. Toro, N. Weiner, and I. Yavin, *High Energy Electron Signals from Dark Matter Annihilation in the Sun*, 0910.1839.
 - [20] P. Meade, S. Nussinov, M. Papucci, and T. Volansky, *Searches for Long Lived Neutral Particles*, 0910.4160.
 - [21] P.-f. Yin and S.-h. Zhu, *Detecting light long-lived particle produced by cosmic ray*, 0911.3338.
 - [22] R. Essig, N. Sehgal, and L. E. Strigari, *Bounds on Cross-sections and Lifetimes for Dark Matter Annihilation and Decay into Charged Leptons from Gamma-ray Observations of Dwarf Galaxies*, 0902.4750.
 - [23] S. Galli, F. Iocco, G. Bertone, and A. Melchiorri, *CMB constraints on Dark Matter models with large annihilation cross-section*, *Phys. Rev.* **D80** (2009) 023505, [0905.0003].
 - [24] T. R. Slatyer, N. Padmanabhan, and D. P. Finkbeiner, *CMB Constraints on WIMP Annihilation: Energy Absorption During the Recombination Epoch*, *Phys. Rev.* **D80** (2009) 043526, [0906.1197].
 - [25] R. Essig, N. Sehgal, L. Strigari, M. Geha, and J. Simon, *Indirect Dark Matter Detection with Segue 1*, *to appear*.
 - [26] <http://hallaweb.jlab.org/parity/prex/>.
 - [27] M. Pospelov, *Secluded $U(1)$ below the weak scale*, 0811.1030.
 - [28] **BABAR** Collaboration, B. Aubert *et al.*, *Search for Dimuon Decays of a Light Scalar in Radiative Transitions $Y(3S) \rightarrow \gamma$ gamma A_0* , 0902.2176.
 - [29] J. D. Bjorken *et al.*, *Search for Neutral Metastable Penetrating Particles Produced in the SLAC Beam Dump*, *Phys. Rev.* **D38** (1988) 3375.
 - [30] E. M. Riordan *et al.*, *A Search for Short Lived Axions in an Electron Beam Dump Experiment*, *Phys. Rev. Lett.* **59** (1987) 755.
 - [31] A. Bross *et al.*, *A Search for Shortlived Particles Produced in an Electron Beam Dump*, *Phys. Rev. Lett.* **67** (1991) 2942–2945.
 - [32] M. J. Strassler, *Possible effects of a hidden valley on supersymmetric phenomenology*, **hep-ph/0607160**.
 - [33] M. J. Strassler and K. M. Zurek, *Echoes of a hidden valley at hadron colliders*, *Phys. Lett.* **B651** (2007) 374–379, [hep-ph/0604261].
 - [34] M. J. Strassler, *Why Unparticle Models with Mass Gaps are Examples of Hidden Valleys*, 0801.0629.
 - [35] K. R. Dienes, C. F. Kolda, and J. March-Russell, *Kinetic mixing and the supersymmetric gauge hierarchy*, *Nucl. Phys.* **B492** (1997) 104–118, [hep-ph/9610479].
 - [36] S. A. Abel and B. W. Schofield, *Brane-antibrane kinetic mixing, millicharged particles and SUSY breaking*, *Nucl. Phys.* **B685** (2004) 150–170, [hep-th/0311051].
 - [37] S. A. Abel, M. D. Goodsell, J. Jaeckel, V. V. Khoze, and A. Ringwald, *Kinetic Mixing of the Photon with Hidden $U(1)$ s in String Phenomenology*, *JHEP* **07** (2008) 124, [0803.1449].

- [38] A. Ringwald, *From Axions to Other WISPs*, 0810.3106.
- [39] Y. Nomura and J. Thaler, *Dark Matter through the Axion Portal*, 0810.5397.
- [40] J. Mardon, Y. Nomura, and J. Thaler, *Cosmic Signals from the Hidden Sector*, 0905.3749.
- [41] N. Arkani-Hamed and N. Weiner, *LHC Signals for a SuperUnified Theory of Dark Matter*, *JHEP* **12** (2008) 104, [0810.0714].
- [42] C. Cheung, J. T. Ruderman, L.-T. Wang, and I. Yavin, *Kinetic Mixing as the Origin of Light Dark Scales*, 0902.3246.
- [43] D. E. Morrissey, D. Poland, and K. M. Zurek, *Abelian Hidden Sectors at a GeV*, 0904.2567.
- [44] A. Katz and R. Sundrum, *Breaking the Dark Force*, 0902.3271.
- [45] **WMAP Collaboration**, E. Komatsu *et al.*, *Five-Year Wilkinson Microwave Anisotropy Probe (WMAP) Observations: Cosmological Interpretation*, *Astrophys. J. Suppl.* **180** (2009) 330–376, [0803.0547].
- [46] **SDSS Collaboration**, D. J. Eisenstein *et al.*, *Detection of the Baryon Acoustic Peak in the Large-Scale Correlation Function of SDSS Luminous Red Galaxies*, *Astrophys. J.* **633** (2005) 560–574, [astro-ph/0501171].
- [47] **Supernova Cosmology Project Collaboration**, S. Perlmutter *et al.*, *Measurements of Omega and Lambda from 42 High-Redshift Supernovae*, *Astrophys. J.* **517** (1999) 565–586, [astro-ph/9812133].
- [48] **Supernova Search Team Collaboration**, A. G. Riess *et al.*, *Observational Evidence from Supernovae for an Accelerating Universe and a Cosmological Constant*, *Astron. J.* **116** (1998) 1009–1038, [astro-ph/9805201].
- [49] **Supernova Cosmology Project Collaboration**, M. Kowalski *et al.*, *Improved Cosmological Constraints from New, Old and Combined Supernova Datasets*, *Astrophys. J.* **686** (2008) 749–778, [0804.4142].
- [50] **PAMELA Collaboration**, O. Adriani *et al.*, *Observation of an anomalous positron abundance in the cosmic radiation*, 0810.4995.
- [51] **The Fermi LAT Collaboration**, A. A. Abdo *et al.*, *Measurement of the Cosmic Ray e^+ plus e^- spectrum from 20 GeV to 1 TeV with the Fermi Large Area Telescope*, 0905.0025.
- [52] J. Chang *et al.*, *An excess of cosmic ray electrons at energies of 300.800 GeV*, *Nature* **456** (2008) 362–365.
- [53] **H.E.S.S. Collaboration**, F. Aharonian *et al.*, *The energy spectrum of cosmic-ray electrons at TeV energies*, *Phys. Rev. Lett.* **101** (2008) 261104, [0811.3894].
- [54] **H.E.S.S. Collaboration**, F. Aharonian, *Probing the ATIC peak in the cosmic-ray electron spectrum with H.E.S.S.*, 0905.0105.
- [55] D. P. Finkbeiner, *Microwave ISM Emission Observed by WMAP*, *Astrophys. J.* **614** (2004) 186–193, [astro-ph/0311547].
- [56] G. Dobler, D. P. Finkbeiner, I. Cholis, T. R. Slatyer, and N. Weiner, *The Fermi Haze: A Gamma-Ray Counterpart to the Microwave Haze*, 0910.4583.
- [57] N. Arkani-Hamed, D. P. Finkbeiner, T. R. Slatyer, and N. Weiner, *A Theory of Dark Matter*, *Phys. Rev.* **D79** (2009) 015014, [0810.0713].
- [58] J. Hisano, S. Matsumoto, and M. M. Nojiri, *Explosive dark matter annihilation*, *Phys. Rev. Lett.* **92** (2004) 031303, [hep-ph/0307216].
- [59] J. March-Russell, S. M. West, D. Cumberbatch, and D. Hooper, *Heavy Dark Matter Through the Higgs Portal*, *JHEP* **07** (2008) 058, [0801.3440].
- [60] M. Cirelli, M. Kadastik, M. Raidal, and A. Strumia, *Model-independent implications of the e^+ , e^- , anti-proton cosmic ray spectra on properties of Dark Matter*, *Nucl. Phys.* **B813** (2009) 1–21, [0809.2409].
- [61] I. Cholis, G. Dobler, D. P. Finkbeiner, L. Goodenough, and N. Weiner, *The Case for a 700+ GeV WIMP: Cosmic Ray Spectra from ATIC and PAMELA*, 0811.3641.
- [62] I. Cholis, D. P. Finkbeiner, L. Goodenough, and N. Weiner, *The PAMELA Positron Excess from Annihilations into a Light Boson*, 0810.5344.
- [63] Y. Cui, D. E. Morrissey, D. Poland, and L. Randall, *Candidates for Inelastic Dark Matter*, *JHEP* **05** (2009) 076, [0901.0557].
- [64] A. Sommerfeld *Ann. Phys.* **11** (1931) 257.
- [65] O. Adriani *et al.*, *A new measurement of the antiproton-to-proton flux ratio up to 100 gev in the cosmic radiation*, 0810.4994.
- [66] D. Alves, S. R. Behbahani, P. Schuster, and J. G. Wacker, *Composite Inelastic Dark Matter*, 0903.3945.
- [67] D. Tucker-Smith and N. Weiner, *Inelastic dark matter*, *Phys. Rev.* **D64** (2001) 043502, [hep-ph/0101138].
- [68] S. Chang, G. D. Kribs, D. Tucker-Smith, and N. Weiner, *Inelastic Dark Matter in Light of DAMA/LIBRA*, 0807.2250.
- [69] R. Bernabei *et al.*, *Dark matter particles in the galactic halo: Results and implications from DAMA/NaI*, *Int. J. Mod. Phys.* **D13** (2004) 2127–2160, [astro-ph/0501412].
- [70] **DAMA Collaboration**, R. Bernabei *et al.*, *First results from DAMA/LIBRA and the combined results with DAMA/NaI*, *Eur. Phys. J.* **C56** (2008) 333–355, [0804.2741].
- [71] A. W. Strong *et al.*, *Gamma-ray continuum emission from the inner Galactic region as observed with INTEGRAL/SPI*, *Astron. Astrophys.* **444** (2005) 495, [astro-ph/0509290].
- [72] D. P. Finkbeiner and N. Weiner, *Exciting Dark Matter and the INTEGRAL/SPI 511 keV signal*, *Phys. Rev.* **D76** (2007) 083519, [astro-ph/0702587].
- [73] **Muon G-2 Collaboration**, G. W. Bennett *et al.*, *Final report of the muon E821 anomalous magnetic moment measurement at BNL*, *Phys. Rev.* **D73** (2006) 072003, [hep-ex/0602035].
- [74] **HyperCP Collaboration**, H. Park *et al.*, *Evidence for the decay $\Sigma^+ \rightarrow p \mu^+ \mu^-$* , *Phys. Rev. Lett.* **94** (2005) 021801, [hep-ex/0501014].
- [75] **The BABAR Collaboration**, B. Aubert, *Search for Dimuon Decays of a Light Scalar in Radiative Transitions $Y(3S) \rightarrow \gamma A0$* , 0902.2176.
- [76] **KTeV Collaboration**, E. Abouzaid *et al.*, *Measurement of the rare decay $\pi^0 \rightarrow e^+ e^-$* , *Phys. Rev.* **D75** (2007) 012004, [hep-ex/0610072].
- [77] Bossi, F., private communication.
- [78] K. J. Kim and Y.-S. Tsai, *Improved Weissäcker-Williams method and its application to lepton and W-boson pair productions*, *Phys. Rev.* **D8** (1973) 3109.
- [79] Y.-S. Tsai, *Pair Production and Bremsstrahlung of Charged Leptons*, *Rev. Mod. Phys.* **46** (1974) 815.
- [80] Y.-S. Tsai, *Axion Bremsstrahlung by and electron beam*, *Phys. Rev.* **D34** (1986) 1326.
- [81] **Particle Data Group Collaboration**, C. Amsler *et al.*,

- Review of particle physics*, *Phys. Lett.* **B667** (2008) 1.
- [82] *NIM A522* **A522** (2004) 294–346.
 - [83] P. Perez and A. Rosowsky *NIM* **A532** (2004) 523.
 - [84] J. Alwall *et al.*, *MadGraph/MadEvent v4: The New Web Generation*, *JHEP* **09** (2007) 028, [[0706.2334](#)].
 - [85] D. Wiser *Ph.D. thesis*, *University of Wisconsin* (1977).
 - [86] E04-012 (<http://hallaweb.jlab.org/experiment/E04-012/>), Y. Qiang, private communication.
 - [87] Note that our estimate of the constraint here disagrees

with those previously published in [3, 7] and [4]. Compared to the published versions of [3, 7], we have here included R and also corrected an error which made the old estimates in [3, 7] too optimistic. The estimate of [4] is also too optimistic, since it did not include the signal efficiency from using one-sigma (mass resolution) bin-widths, and it also used an overly optimistic mass resolution for BaBar.